

The impact of UV variability on the abundance of bright galaxies at $z \geq 9$

Xuejian Shen,^{1,2*} Mark Vogelsberger,² Michael Boylan-Kolchin,³ Sandro Tacchella,^{4,5} and Rahul Kannan⁶

¹ TAPIR, California Institute of Technology, Pasadena, CA, 91125

² Department of Physics & Kavli Institute for Astrophysics and Space Research, Massachusetts Institute of Technology, Cambridge, MA 02139, USA

³ Department of Astronomy, The University of Texas at Austin, 2515 Speedway Stop C1400, Austin, TX 78712, USA

⁴ Kavli Institute for Cosmology, University of Cambridge, Madingley Road, Cambridge, CB3 0HA, UK

⁵ Cavendish Laboratory, University of Cambridge, 19 JJ Thomson Avenue, Cambridge, CB3 0HE, UK

⁶ Department of Physics and Astronomy, York University, 4700 Keele Street, Toronto, ON M3J 1P3, Canada

Accepted XXX. Received YYY; in original form ZZZ

ABSTRACT

JWST observations have revealed a population of galaxies bright enough that potentially challenge standard galaxy formation models in the Λ CDM cosmology. Using a minimal empirical framework, we investigate the influence of variability on the rest-frame ultra-violet (UV) luminosity function (UVLF) of galaxies at $z \geq 9$. Our study differentiates between the *median UV radiation yield* and the *variability of UV luminosities* of galaxies at a fixed dark matter halo mass. We primarily focus on the latter effect, which depends on halo assembly and galaxy formation processes and can significantly increase the abundance of UV-bright galaxies due to the upscatter of galaxies in lower-mass haloes. We find that a relatively low level of variability, $\sigma_{UV} \approx 0.75$ mag, matches the observational constraints at $z \approx 9$. However, increasingly larger σ_{UV} is necessary when moving to higher redshifts, reaching $\sigma_{UV} \approx 2.0$ (2.5) mag at $z \approx 12$ (16). This implied variability is consistent with expectations of physical processes in high-redshift galaxies such as bursty star formation and dust clearance during strong feedback cycles. Photometric constraints from JWST at $z \geq 9$ therefore can be reconciled with a standard Λ CDM-based galaxy formation model calibrated at lower redshifts without the need for adjustments to the median UV radiation yield.

Key words: galaxies: high-redshift – galaxies: formation – galaxies: evolution

1 INTRODUCTION

The James Webb Space Telescope (JWST) has opened a new window into the early and distant Universe, enabling studies of galaxy formation and evolution within the first ~ 500 Myr ($z \gtrsim 10$) of the age of the Universe. Early JWST/NIRCam imaging datasets have led to the discovery of numerous photometric drop-out galaxy candidates at $z \gtrsim 9$ (e.g. Naidu et al. 2022b; Castellano et al. 2022; Finkelstein et al. 2022; Adams et al. 2023b; Atek et al. 2023; Bouwens et al. 2023a; Donnan et al. 2023; Harikane et al. 2023b; Robertson et al. 2023; Yan et al. 2023) and even unusually bright galaxy candidates at $z \approx 16$ (Donnan et al. 2023; Harikane et al. 2023b).

The UV luminosities and estimated stellar masses of these sources have raised two key tensions. The first tension is related to the large stellar mass of some JWST-identified galaxies (e.g. Labbé et al. 2023), implying that the stellar mass density at $z \approx 7.5 - 9$ is comparable to the total mass budget of baryons within sufficiently massive dark matter haloes in a Λ CDM universe (Boylan-Kolchin 2023; Lovell et al. 2023). This result has been actively debated in the literature and is subject to many systematic uncertainties (e.g. Endsley et al. 2023; Larson et al. 2022; Steinhardt et al. 2023; Chen et al. 2023; Prada et al. 2023). The stellar masses and star-formation rates (SFRs) of individual galaxies at $z \gtrsim 10$ thus far appear consistent

with the standard structure formation theory (e.g. Keller et al. 2023; McCaffrey et al. 2023).

The second tension concerns the abundance of UV bright galaxies, which is more robust and will be the focus of this paper. Although characteristic shapes of the rest-frame UV luminosity functions (UVLFs) determined using JWST-identified galaxies are consistent with those derived with the Hubble Space Telescope (HST) observations, the bright end of the UVLFs shows little evolution beyond $z \approx 10$ and lacks the steep decline expected from extrapolating Schechter function fits from lower redshifts (e.g. Harikane et al. 2023b; Finkelstein et al. 2023). As a result, the implied star-formation rate density (SFRD) declines only slowly at $z \gtrsim 10$, in contrast to the rapid decline predicted by constant star-formation efficiency models (e.g. Bouwens et al. 2023b; Harikane et al. 2023b).

Even after accounting for various observational corrections (e.g. Finkelstein et al. 2023), the suggested abundance of UV bright galaxies at $z \gtrsim 10$ surpasses theoretical predictions from a wide range of models. This includes empirical models (e.g. Tacchella et al. 2013; Mason et al. 2015; Sun & Furlanetto 2016; Tacchella et al. 2018; Behroozi et al. 2020), semi-analytical galaxy formation models (e.g. Dayal et al. 2014, 2019; Yung et al. 2019; Mauerhofer & Dayal 2023; Yung et al. 2023), and cosmological hydrodynamic simulations (e.g. Davé et al. 2019; Vogelsberger et al. 2020; Haslbauer et al. 2022; Kannan et al. 2022, 2023; Wilkins et al. 2023b,a) that have been calibrated for lower redshift galaxies. One possible explanation for this discrepancy is that the early results are based on the

* E-mail: xshen@caltech.edu

photometrically-selected galaxy candidates, which may be contaminated by low-redshift interlopers (e.g. Zavala et al. 2023; Naidu et al. 2022a; Fujimoto et al. 2022). However, recent pure spectroscopic constraints of the UVLF (e.g. Arrabal Haro et al. 2023a,b; Curtis-Lake et al. 2023; Robertson et al. 2023; Harikane et al. 2023a) yield broadly consistent results with the photometric estimates.

The UVLF tension between observations and predictions suggests that our current understanding of galaxy formation in the early Universe may need to be revised. Several physical interpretations have been discussed in the literature to explain the tension (e.g. Inayoshi et al. 2022; Ferrara et al. 2023; Dekel et al. 2023; Mason et al. 2023; Yung et al. 2023). These include but are not limited to (1) a substantially higher star-formation efficiency for normal stellar populations, (2) a top-heavy stellar initial mass function (IMF), (3) zero dust attenuation, (4) UV radiation contributed by non-stellar sources, e.g. accreting stellar-mass black holes, quasars/active galactic nuclei. These solutions primarily aim to enhance the *median* UV radiation yield from early galaxies. Another direction suggested by e.g. Mason et al. (2023) and Mirocha & Furlanetto (2023) involves increased stochasticity of star formation such that galaxies in a temporary high-SFR phase will appear as the UV luminous sources. The steep decline of the underlying halo mass function in the massive/bright end means that there are more intrinsically low-mass sources upscattered to high luminosities than massive galaxies downscattered to faint luminosities, which will populate the bright end of the UVLF.

In this paper, we examine the UV variability of high-redshift galaxies coming from a variety of sources of stochasticity, including halo assembly, star formation, and dust attenuation, in the context of a canonical Salpeter (1955) IMF. We investigate the impact of UV variability on galaxy UVLFs, focusing on the constraints imposed by JWST observations at $z \geq 9$. We will study this using an empirical approach and decompose the effects of variability and the shift of the median galaxy-halo connection. The paper is organized as follows: In Section 2, we first introduce the model establishing a median mapping between the halo mass function and galaxy UVLF. We then describe how we treat UV variability. In Section 3, we present the results and discuss the implication of UV variability in reconciling JWST observations with a standard galaxy formation model in Λ CDM. In Section 4, we provide our conclusions.

2 METHOD

2.1 Median galaxy UV luminosity

We adopt the flat Λ CDM cosmological model of Planck Collaboration et al. (2020), assuming the primordial density fluctuations are Gaussian and adiabatic. The cosmological parameters relevant for this study are $h \equiv H_0/(100 \text{ km s}^{-1} \text{ Mpc}^{-1}) = 0.6732$, $\Omega_m = 0.3158$, $n_s = 0.96605$, $\sigma_8 = 0.8120$, and $f_b \equiv \Omega_b/\Omega_m = 0.156$.

Halo mass function: The halo mass function is constructed following Press-Schechter-like theories (e.g. Press & Schechter 1974; Bond et al. 1991; Sheth et al. 2001) as implemented in the HMF code (Murray et al. 2013; Murray 2014). We adopt the transfer function calculated using the Code for Anisotropies in the Microwave Background (CAMB; Lewis et al. 2000; Howlett et al. 2012), the halo mass function parametrization of Tinker et al. (2010), and a real-space top-hat filter function for the density field. The definition of halo mass follows the virial criterion in Bryan & Norman (1998).

Halo accretion rate: We use the fitting function of *median* halo

accretion rate in Fakhouri et al. (2010)

$$\dot{M}_{\text{halo}}(M_{\text{halo}}, z) \simeq 25.3 M_{\odot} \text{ yr}^{-1} \left(\frac{M_{\text{halo}}}{10^{12} M_{\odot}} \right)^{1.1} \times (1 + 1.65z) \sqrt{\Omega_m (1+z)^3 + \Omega_{\Lambda}}, \quad (1)$$

which is calibrated on the joint data set from the Millennium and Millennium-II simulations (Springel et al. 2005; Boylan-Kolchin et al. 2009)¹.

Star formation: We parameterize the SFR in dark matter haloes as $\text{SFR} = \varepsilon_* f_b \dot{M}_{\text{halo}}$, where f_b is the universal baryon fraction and ε_* is the star-formation efficiency. We adopt a *redshift-independent* double power-law function,

$$\varepsilon_*(M_{\text{halo}}) = \frac{2\varepsilon_0}{(M_{\text{halo}}/M_0)^{-\alpha} + (M_{\text{halo}}/M_0)^{\beta}}, \quad (2)$$

where ε_0 is the peak star-formation efficiency at the characteristic mass M_0 and α and β are the low-mass and high-mass end slopes, respectively. The functional form and the redshift-independent ansatz of Equation 2 have been used in previous empirical modeling works (e.g. Moster et al. 2010; Tacchella et al. 2018; Harikane et al. 2022). We adopt $\varepsilon_0 = 0.1$, $M_0 = 10^{12} M_{\odot}$, $\alpha = 0.6$, $\beta = 0.5$ as our default values. The normalization and low-mass slope are chosen to match the median SFR- M_{halo} relation at $z = 7$ from Behroozi et al. (2019) while the high-mass slope follows the value in Harikane et al. (2022). The parameter choices give good agreement with the observed UVLFs and UV luminosity densities at $z \lesssim 9$. At the halo mass scale that is typical for bright JWST-detected galaxies ($M_{\text{halo}} \sim 10^{10} M_{\odot}$), ε_* takes the value of ~ 0.01 . This model is a basic representation² of our knowledge about galaxy formation prior to the JWST era.

SFR – UV luminosity: We express the conversion between the SFR and the intrinsic UV-specific luminosity $L_{\nu}(\text{UV})$ (before dust attenuation) as

$$\text{SFR} [M_{\odot} \text{ yr}^{-1}] = \kappa_{\text{UV}} L_{\nu}(\text{UV}) [\text{erg s}^{-1} \text{ Hz}^{-1}] \quad (3)$$

with conversion factor $\kappa_{\text{UV}} = 1.15 \times 10^{-28}$ as in Madau & Dickinson (2014), where a Salpeter (1955) IMF is assumed and the (far-)UV wavelength is assumed to be 1500 \AA .

Dust attenuation: We empirically model dust attenuation using a combination of the $A_{\text{UV}}-\beta$ (IRX- β) relation and $\beta-M_{\text{UV}}$ relation. We adopt the relation $A_{\text{UV}} = 4.43 + 1.99\beta$ (Meurer et al. 1999) and the most recent $\beta-M_{\text{UV}}$ relation $\beta = -0.17 M_{\text{UV}} - 5.40$ at $z \gtrsim 8$ from Cullen et al. (2023). Combine the two relations, we obtain a *median* attenuation at a given M_{UV} of

$$A_{\text{UV}} = -0.34 [21 + M_{\text{UV}}] + 0.79. \quad (4)$$

¹ The cosmological parameters adopted in these simulations are out of date. As discussed in Inayoshi et al. (2022), the impact on the halo growth rate is limited ($\lesssim 0.1$ dex), as found in Dong et al. (2022) using up-to-date cosmological parameter sets.

² Star formation in high-redshift galaxies potentially exhibits complex dependencies on numerous factors that are not captured by a straightforward empirical model. There are substantial uncertainties in constraining these factors with available observational data along with strong model dependence in the calibration procedure. Acknowledging these challenges, the main goal of this empirical model is to create a rough reference point, representing models built prior to the introduction of JWST data. Subsequently, we aim to parameterize model variations by the shift in the median galaxy-halo connection with respect to this reference model and variability.

The M_{UV} here is the observed (dust-attenuated) UV magnitude. The recipe gives median $A_{UV} = [0.45, 0.79, 1.13]$ mag attenuation at observed $M_{UV} = [-20, -21, -22]$ mag.

2.2 UV variability

The model above describes a *median* mapping from the dark matter halo mass to the observed galaxy UV luminosity. It allows us to calculate galaxy rest-frame UVLF based on the underlying halo mass function

$$\frac{dn}{dM_{UV}} = \frac{dn}{d \log_{10} M_{\text{halo}}} \left| \frac{d \log_{10} M_{\text{halo}}}{dM_{UV}} \right|. \quad (5)$$

However, stochasticity in both halo assembly and galaxy formation processes can give rise to scatter with respect to the median $M_{UV} - M_{\text{halo}}$ relation. This manifests as the scatter in all scaling relations we introduced above. To model this stochasticity, we convolve the UV luminosity function with a Gaussian kernel³ of width σ_{UV} (in unit of AB magnitude). Effectively, this assumes that the observed UV luminosity has a log-normal distribution with the *median* value fixed. Note that this will increase the *mean* UV luminosity by a factor of

$$\frac{\langle L_V^{\text{conv}}(UV) \rangle}{\langle L_V(UV) \rangle} = \exp\left(\frac{(\ln 10 \sigma_{UV}/2.5)^2}{2}\right), \quad (6)$$

which is equivalent to roughly $0.5 \sigma_{UV}^2$ mag. Moreover, due to the steeply decreasing nature of the halo mass function and the UVLF, the upscatter in UV luminosity dominates over the downscatter, leading to an enhanced abundance of UV luminous galaxies. This effect will be demonstrated and discussed in the results section of the paper. We use the term ‘‘UV variability’’ to summarize this scatter in the $M_{UV} - M_{\text{halo}}$ relation since the variations of luminosities of single sources over short time scales could contribute significantly to the scatter. The potential source of UV variability include:

Halo assembly: The mass accretion rate of dark matter haloes roughly follows a log-normal distribution with a typical 1σ scatter of $\sigma_{\text{halo}} \approx 0.3$ dex, which is broadly consistent with cosmological N -body simulations (e.g. Rodríguez-Puebla et al. 2016; Ren et al. 2019; Mirocha et al. 2021; Mirocha & Furlanetto 2023). It is independent of any baryonic processes.

Star formation: In both simulations and observations, small dwarf galaxies and high-redshift galaxies exhibit ‘‘bursty’’ star-formation histories (e.g. Sparre et al. 2017; Smit et al. 2016; Emami et al. 2019; Iyer et al. 2020; Tacchella et al. 2020; Flores Velázquez et al. 2021; Hopkins et al. 2023) characterized by large temporal fluctuations in SFR. This bursty phase aligns with the irregular and clumpy morphologies of the observed high-redshift galaxies (e.g. Bournaud et al. 2007; Elmegreen et al. 2009; Förster Schreiber et al. 2011; Treu et al. 2023). Large scatter in star-formation efficiency can be driven by the interplay of gas inflow/outflow, instability, and galaxy mergers in the early phase of galaxy formation (e.g. Dekel et al. 2009; Ceverino et al. 2010; Anglés-Alcázar et al. 2017), cycles of starbursts ceased by strong feedback (e.g. El-Badry et al. 2016; Tacchella et al. 2016), and

some extreme feedback-free starbursts (e.g. Faucher-Giguère 2018; Dekel et al. 2023). Galaxies in this phase are qualitatively different from sufficiently massive low-redshift star-forming galaxies in equilibrium stages, which exhibit smooth galaxy-integrated SFRs. The expected SFR variability in high-redshift galaxies is highly uncertain. The lower limit should be the scatter in star-formation efficiency (≈ 0.15 dex) inferred from observations at $z \lesssim 7$ (e.g. Harikane et al. 2018, 2022), and the main sequence scatter at high redshift, ≈ 0.3 dex (Speagle et al. 2014). We conservatively assume $\sigma_{\text{SF}} \geq 0.3$ dex.

Dust attenuation: Given the irregular and clumpy nature of high-redshift galaxies, the sightline and geometrical variations of dust attenuation can be large (e.g. Carniani et al. 2018; Cochrane et al. 2019; Ferrara et al. 2022). In addition, the strong supernovae and radiative feedback, both temporally and spatially associated with the burst phase of star formation, can expel the majority of the cold phase gas and cause galaxies to temporarily become transparent to dust attenuation (e.g. Ferrara et al. 2023; Fiore et al. 2023; Nath et al. 2023; Ziparo et al. 2023). The degree of UV variability contributed or balanced off by these factors depends on the amount of dust in these galaxies as well as the coherence between the dust clearance and the starburst. The scatter in the observed $\beta - M_{UV}$ relation is found to be $\sigma_{\beta} \approx 0.35$ (Bouwens et al. 2014; Rogers et al. 2014; Cullen et al. 2023), which corresponds to $\sigma_{\text{dust}} \approx 0.7$ mag for our assumed $A_{UV} - \beta$ relation.

Bracketing the combined effect: The true UV variability in high-redshift galaxies, as well as its potential dependence on halo mass or redshift, are challenging to constrain given the uncertainties in the physical drivers, the limited observational probes, and errors. Consequently, we maintain it as a free parameter throughout our analysis while adhering to specific constraints. To model the combined effects of the three sources of variability mentioned above, we numerically sample haloes based on the halo mass function and calculate their observed UV magnitudes individually. We model the halo mass accretion rate, \dot{M}_{halo} , and the star formation efficiency, ε_* , as log-normal distributions, while the dust attenuation, A_{UV} , is modeled as a normal distribution. Their median values are determined as in Section 2.1. The 1σ scatters are σ_{halo} , σ_{SF} , and σ_{dust} , as estimated above, and are assumed to be independent of M_{halo} and z . Owing to the influence of dust attenuation (Equation 4), the relationship between M_{UV} and $\log_{10} M_{\text{halo}}$ is non-linear. The distribution of observed UV luminosities for galaxies at a fixed halo mass, therefore, does not strictly follow a log-normal distribution. To define the effective σ_{UV} , we match the numerically sampled UVLF with the one obtained through convolution using Gaussian kernels of width σ_{UV} at $M_{UV} \approx -21$ at $z \approx 10$ (our results are insensitive to these assumed values of M_{UV} and z). We consider three typical cases. (1) If we account for only σ_{halo} while ignoring scatter in ε_* and A_{UV} , we obtain $\sigma_{UV} \approx 0.6$ (0.75) mag with (without) dust attenuation, which sets the minimum UV variability. (2) If the scatters in \dot{M}_{halo} , ε_* , and A_{UV} are perfectly correlated, we obtain $\sigma_{UV} \geq 2.2$ mag, which represents the maximum UV variability. (3) If the scatters in \dot{M}_{halo} , ε_* , and A_{UV} are independent, we obtain $\sigma_{UV} \geq 1.2$ mag, which serves as a more conservative estimate.

3 RESULTS

In Figure 1, we present the UVLF calculated at $z \geq 9$ assuming different levels of UV variability. For comparison, we show the observational constraints based on the photometrically-selected JWST

³ The choice of the convolution kernel here is motivated by the observed or theoretically-predicted distribution of halo accretion rates (e.g. Fakhouri et al. 2010; Ren et al. 2019; Mirocha et al. 2021) and star formation rates of high-redshift galaxies (e.g. Speagle et al. 2014; Popesso et al. 2023; Pallottini & Ferrara 2023), which contribute to the UV variability. The same kernel is adopted in many previous studies that include the variability effects (e.g. Ren et al. 2018; Whitler et al. 2020).

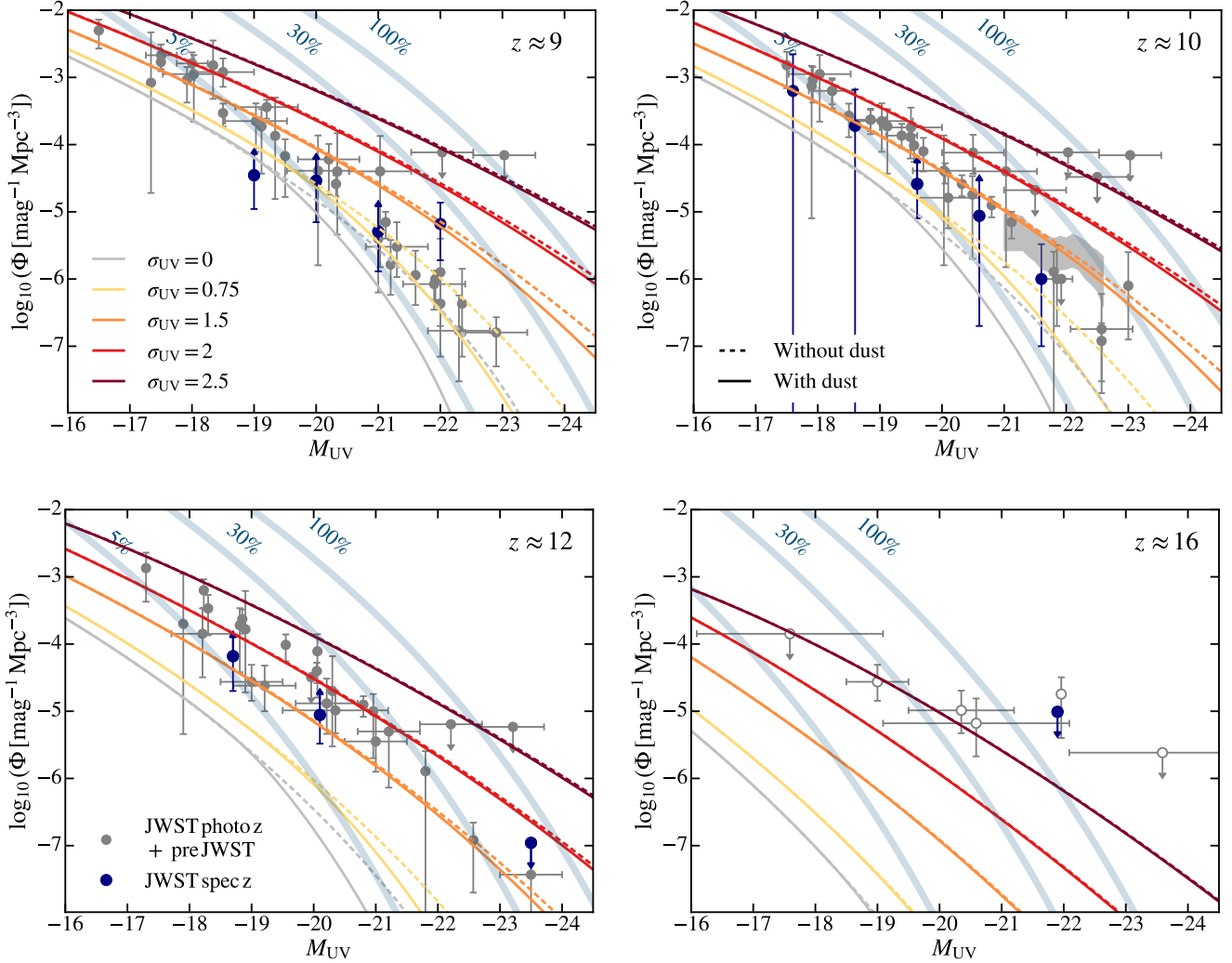


Figure 1. Rest-frame UV luminosity functions (UVLFs) of galaxies at $z \geq 9$. The blue lines represent UVLFs assuming a constant star-formation efficiency ε_* of the value marked. The gray data points are measurements based on photometrically-selected galaxies by JWST (Castellano et al. 2022; Finkelstein et al. 2022; Naidu et al. 2022b; Adams et al. 2023a; Bouwens et al. 2023a,b; Donnan et al. 2023; Harikane et al. 2023b; Leethochawalit et al. 2023; McLeod et al. 2023; Morishita & Stiavelli 2023; Pérez-González et al. 2023) as well as pre-JWST constraints (McLeod et al. 2016; Oesch et al. 2018; Morishita et al. 2018; Stefanon et al. 2019; Bowler et al. 2020; Bouwens et al. 2021). The photometric constraints at $z \approx 16$ are highly uncertain and therefore shown with open markers. The dark blue data points are based on the JWST spectroscopically-confirmed galaxies (e.g. Arrabal Haro et al. 2023a,b; Bunker et al. 2023; Curtis-Lake et al. 2023; see the full references in Harikane et al. 2023a). Assuming our default halo-mass-dependent ε_* (Equation 2), UV variability of $\sigma_{UV} \approx 1.5, 2.0, 2.5$ mag is required to match the JWST photometric constraints at $z \approx 10, 12, 16$. At $z \approx 9$, a lower value of 0.75 mag is preferred to match observations at the bright end.

sources (Castellano et al. 2022; Finkelstein et al. 2022; Naidu et al. 2022b; Adams et al. 2023a; Bouwens et al. 2023a,b; Donnan et al. 2023; Harikane et al. 2023b; Leethochawalit et al. 2023; McLeod et al. 2023; Morishita & Stiavelli 2023; Pérez-González et al. 2023), pre-JWST constraints (McLeod et al. 2016; Oesch et al. 2018; Morishita et al. 2018; Stefanon et al. 2019; Bowler et al. 2020; Bouwens et al. 2021), and the constraints based on pure spectroscopically-confirmed samples compiled in Harikane et al. (2023a). We note that the $z \approx 16$ constraints are based on a few photometrically-selected galaxy candidates and therefore highly uncertain. For example, one previously-claimed $z \approx 16$ galaxy candidate first identified in Donnan et al. (2023) was found to be a galaxy at $z = 4.912$ (Arrabal Haro et al. 2023b). In addition, at $z \approx 10, 12$, the photometric redshifts of galaxy candidates have non-negligible scatter (e.g. Finkelstein et al. 2023; McLeod et al. 2023). A safer way to approach the problem is

to consider the full redshift probability distribution for each galaxy candidate when constructing the UVLF, but it is beyond the scope of this study.

Models with a constant star-formation efficiency and zero UV variability require $\varepsilon_* \geq 30\%$ to explain the most stringent observational results at $z \geq 10$, which is much higher than the canonical value $\varepsilon_* \lesssim 5\%$ for $z \lesssim 9$ galaxies in a similar mass range. Such models also fail to reproduce the shape of observed UVLFs: they have steeper faint-end slopes and more abrupt exponential cutoffs than observations. Adopting the halo mass-dependent star-formation efficiency $\varepsilon_*(M_{\text{halo}})$ from Equation 2 helps make the shape of the UVLF more consistent with observations. Nevertheless, in the absence of UV variability, the model systematically underpredicts the luminosity of galaxies. Using $\sigma_{UV} = 0.75$ mag, our assumed minimum value (coming solely from scatter in halo accretion rates), leads to a UVLF

that is consistent with the $z = 9$ observational results at the bright end. Similar value has been found in previous studies (e.g. Ren et al. 2018; Ren et al. 2019; Whitler et al. 2020). At the faint end at $z = 9$, a larger $\sigma_{UV} \approx 1.5$ mag is required. This is a general trend at all redshifts studied, which is consistent with low-mass galaxies having more bursty star formation. However, we caution that any mass or luminosity dependence of σ_{UV} may be degenerate with assumptions about the explicit halo mass dependence of ε_* (i.e., smaller values of α in Equation 2).

As the UV variability increases, the abundance of luminous galaxies is enhanced. $\sigma_{UV} = 1.5, 2.0, 2.5$ mag is sufficient to explain current JWST constraints at $z = 10, 12, 16$, even assuming *all* photometrically-selected candidates are real. This level of UV variability can be contributed by additional variances in star-formation efficiency and dust attenuation, with potentially large correlations with the variation of halo accretion rates (as discussed in Section 2.2). Similar values tend to overproduce galaxies at $z \leq 9$, indicating a qualitative transition in UV variability at $z \approx 10$. These UV-bright phase galaxies are expected to have very blue intrinsic colors in UV (e.g. Topping et al. 2022; Adams et al. 2023b; Atek et al. 2023; Cullen et al. 2023) but could be balanced by dust attenuation (Mirocha & Furlanetto 2023), depending on how aligned the dust and the star-formation duty-cycles are. Considering the small fields probed by JWST, cosmic variance due to large-scale galaxy clustering could be significant. We refer to the estimates in Yung et al. (2023) using the online calculator of Trenti & Stiavelli (2008). For typical effective survey areas of JWST ($\approx 10 - 35$ arcmin²) at $z \gtrsim 10$, the cosmic variance is ≤ 0.2 dex in number density, which is subdominant compared to other observational uncertainties. Increasing UV variability will further decrease cosmic variance since the observed galaxies will correspond to lower-mass haloes, which are less clustered.

The UV variability has a stronger influence on the bright end of the UVLF. However, integrated down to a canonical faint-end limit $M_{UV} \approx -18$ to -17 (e.g. Bouwens et al. 2015; McLeod et al. 2016; Oesch et al. 2018; Bouwens et al. 2020; Harikane et al. 2023b), it still has a substantial impact. In the top panel of Figure 2, we show the UV luminosity density integrated down to $M_{UV} = -18$ (lower boundary of each shaded region) and $M_{UV} = -17$ (upper boundary) as a function of redshift. They are compared to observational constraints (Coe et al. 2013; Ellis et al. 2013; Bouwens et al. 2020, 2023a,b; Donnan et al. 2023; McLeod et al. 2023; Harikane et al. 2023b; Pérez-González et al. 2023). The measurements based on spectroscopically-confirmed samples from Harikane et al. (2023a) are shown in blue. A low value of σ_{UV} between 0.75 and 1.5 mag works reasonably well in explaining the ρ_{UV} (and similarly for SFR density) at $z \lesssim 10$. A clear transition happens at $z \gtrsim 10$, where a larger UV variability $\sigma_{UV} \gtrsim 1.5$ mag is necessary to explain observational results if one maintains the same median galaxy-halo connection. In the bottom panel of Figure 2, we show the cosmic stellar mass density by integrating the SFR density from $z = 20$. The SFR density is converted from the UV luminosity density using Equation 3, assuming the same limiting magnitude range. We highlight a redshift-dependent σ_{UV} scenario, where a large $\sigma_{UV} \approx 2.5$ mag at $z \approx 16$ declines to $\approx 0.75 - 1.5$ mag at $z \approx 10$. We compared these results with the latest observational constraints compiled in Papovich et al. (2023) and the predictions from the UCHUU-UM model (Prada et al. 2023). We find the large UV variability at high redshift does not lead to any discrepancies with the stellar mass density constraints at $z \lesssim 10$.

To illustrate the implication of UV variability in reconciling JWST results with theoretical models, in Figure 3, we examine the parameter space of UV variability and the median UV radiation yield. For

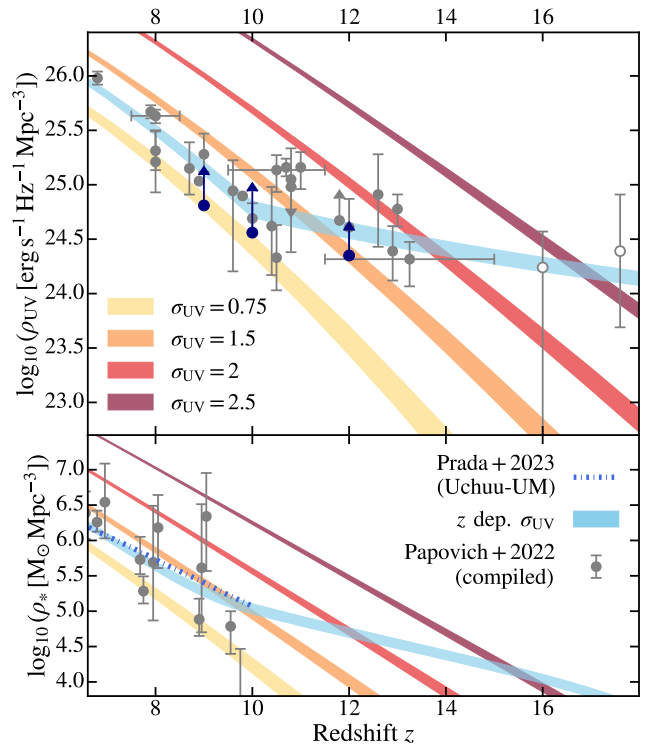


Figure 2. *Top panel:* UV luminosity density ρ_{UV} of galaxies, integrated down to $M_{UV} = -18$ (lower boundary of each shaded region) and $M_{UV} = -17$ (upper boundary), as a function of redshift. The gray data points show photometric constraints (Coe et al. 2013; Ellis et al. 2013; Bouwens et al. 2020, 2023a,b; Donnan et al. 2023; McLeod et al. 2023; Harikane et al. 2023b; Pérez-González et al. 2023) while the dark blue ones highlight pure spectroscopic constraints from Harikane et al. (2023a). At $z \lesssim 10$, a relatively low UV variability — comparable to what is expected solely from variance in halo accretion rates — is sufficient to explain the observations. At $z \gtrsim 10$, an increasingly large UV variability is required to explain the observational results. The cyan line shows a redshift-dependent σ_{UV} inferred from our comparison with JWST UVLFs (declining from $\sigma_{UV} \approx 2.5$ mag at $z \approx 16$ to $\approx 0.75 - 1.5$ mag at $z \lesssim 10$). *Bottom panel:* The cosmic stellar mass density obtained by integrating the SFR density from $z = 20$, assuming the same limiting magnitude range. The results are compared with the latest observational constraints compiled in Papovich et al. (2023) and the predictions from the UCHUU-UM model (Prada et al. 2023). The cyan line shows the results assuming the redshift-dependent σ_{UV} . The large σ_{UV} at early times does not lead to any discrepancies with the stellar mass density constraints at $z \lesssim 10$.

results based on JWST spectroscopy, we consider the model to be consistent with observations when $\log_{10} \Phi(M_{UV} = -20.5) > -5$ and -5.3 at $z=10$ and 12 , respectively. For photometric constraints, we consider the model to be acceptable when $\log_{10} \Phi(M_{UV} = -20.5) > -4.7, -5.0$ and -5.2 at $z=10, 12$ and 16 , respectively. We scan the parameter space by modifying UV variability and the normalization ε_0 of the star-formation efficiency in our model and identify the regime where theoretically predicted UV bright galaxy abundance exceeds the observed values.

As illustrated in the figure, there are two ways to reconcile the model with the JWST results. One option is to enhance the *median* UV radiation yield, either by boosting the star-formation efficiency or enhancing the UV radiation efficiency. For example, the κ_{UV} can drop significantly if assuming different IMFs. For a Chabrier (2003) IMF, κ_{UV} can drop by roughly 37% (Madau & Dickinson 2014). For an extremely top-heavy IMF that may be appropriate for, e.g., metal-free

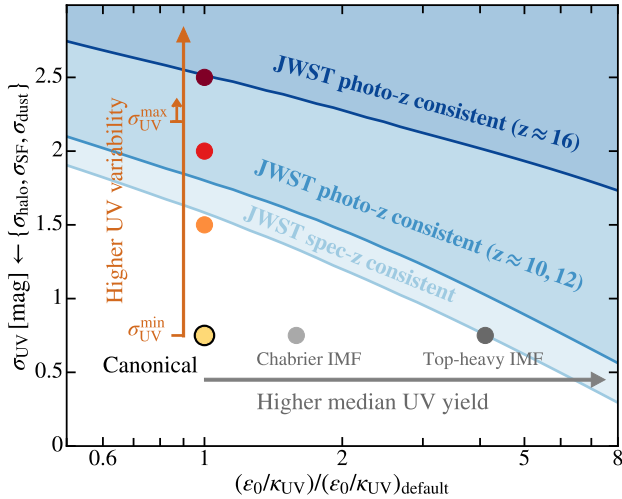


Figure 3. Parameter space of UV variability, σ_{UV} , versus median UV radiation yield, represented by ϵ_0/κ_{UV} . The shaded regions show the regions of parameter space consistent with the JWST results mapped by our empirical model. This parametrization highlights two distinct ways of easing the current tension between theoretical models and observations: enhancing the median UV radiation yield or enhancing the UV variability. The minimum and maximum σ_{UV} estimated in Section 2.2 are shown. Reasonable values of σ_{UV} within the constraints can explain the most stringent JWST results. In the horizontal direction, we show the enhancement of median UV radiation yield for e.g. two alternative IMFs.

Population III stars, κ_{UV} can drop by 76%, to 0.28×10^{-28} (Inayoshi et al. 2022). These scenarios are indicated by the gray dots in the figure. However, this approach can not reconcile the most stringent JWST photometric constraints at $z \approx 16$. An alternative approach is to enhance the variability in the observed UV luminosity, as highlighted by the colored dots and explored in more detail in earlier figures. In this paper, we have focused on the latter option and assumed a log-normal distribution of observed UV luminosity. However, in practice, a similar phenomenon can be driven by e.g. incorporating a fraction of starbursts with high star-formation efficiencies.

4 DISCUSSION AND CONCLUSIONS

In this paper, we study the impact of UV variability on the rest-frame UVLF of galaxies at $z \geq 9$ constrained by recent JWST observations. We introduce an empirical model that links host dark matter halo mass to the median galaxy UV luminosity and make predictions for the UVLF at high redshift. This model is designed to minimize dependence or assumptions on specific galaxy formation recipes and represent our understanding of galaxy formation prior to the JWST era. Based on this *median* galaxy-halo connection, we investigate the extent of UV variability required to explain the substantial presence of UV-bright galaxies observed by JWST at $z \geq 9$. This UV variability encompasses the random fluctuations in halo assembly, star formation, and dust attenuation processes.

Even assuming *all* the photometrically-selected candidates are real, we find that JWST observations at $z \approx 10, 12, 16$ can be reconciled with a standard galaxy formation model calibrated at low redshift with $\sigma_{UV} \approx 1.5, 2.0, 2.5$ mag. Our results indicate a transition at $z = 10$. Below this redshift, $\sigma_{UV} \approx 0.75 - 1.5$ mag is favored to match the UVLF and the cumulative UV luminosity den-

sity of the Universe. At higher redshifts, the required value of σ_{UV} is larger and grows with increasing redshift in order to reproduce the bright end of the UVLF. This transition implies a sharp change in the underlying mechanism that is responsible for the observed UV variability. UV emission is sensitive to the SFR over a time scale of $\sim 10 - 100$ Myr (e.g. Murphy et al. 2011; Flores Velázquez et al. 2021), close to the dynamical timescale of a dark matter halo in virial equilibrium — which sets the time scale of baryon cycles in high-redshift galaxies — at $z \approx 10$ (e.g. Anglés-Alcázar et al. 2017; Tacchella et al. 2020). In addition, the characteristic redshift could correspond to the epoch when the cooling and free-fall time in dense gas disks becomes shorter than the time for low-metallicity massive stars to develop winds and supernovae (\sim Myr; Faucher-Giguère 2018; Dekel et al. 2023). This scenario is explicitly studied in Dekel et al. (2023), who found that feedback-free starburst with high star-formation efficiencies can occur at $z \gtrsim 10$.

The implied UV variability is consistent with the expected values from halo assembly, burstiness of star formation in high-redshift galaxies, and dust attenuation variations. In addition to using UV as the primary tracer, emission line measurements (e.g. $H\gamma$ and $H\delta$ using JWST NIRSpec, $H\alpha$ using JWST MIRI) for $z \approx 10$ galaxies will be useful in measuring the burstiness of star formation from, e.g., the ratio of $H\alpha$ versus UV luminosity (e.g. Broussard et al. 2019; Caplar & Tacchella 2019; Emami et al. 2019; Faisst et al. 2019; Iyer et al. 2022) and isolate the physical origin of the burstiness. These emission line tracers are sensitive to SFR as measured on very short time scales and are therefore useful for studying processes such as the feedback-free starbursts highlighted above and the typical lifecycle of giant molecular clouds ($\lesssim 10$ Myr; e.g. Leitherer et al. 1999; Tan 2000; Tasker 2011). High-resolution hydrodynamical simulations with **predictive power** below the interstellar medium (ISM) scale will also shed light on the physical origin of UV variability and its implication for resolving the UVLF tension (Pallottini & Ferrara 2023; Sun et al. 2023).

In summary, current theoretical frameworks such as empirical models, semi-analytical models, and large-volume numerical simulations might substantially underestimate the variability in UV luminosity of individual galaxies arising from various baryonic physics processes at or below the interstellar medium scale (e.g. Iyer et al. 2020; Tacchella et al. 2020) in the extremely high-density environment at high redshift. These models underestimate the observed UVLF at high redshift unless they adopt an increase in the median UV radiation yield. However, by incorporating a physically motivated higher UV variability, the need for adjustments to a standard galaxy formation model — such as introducing a top-heavy stellar initial mass function, a drastically different star-formation law, or considering significant contamination from non-stellar sources — can be substantially reduced. As a result, the bright galaxy populations unveiled by JWST at $z \gtrsim 10$ are consistent with the Λ CDM cosmological model paired with a standard galaxy formation model, assuming a reasonable variability in UV luminosity.

ACKNOWLEDGEMENTS

We thank Josh Borrow, Rohan Naidu, Anna-Christina Eilers, Claude-André Faucher-Giguère, Guochao Sun, and Christopher Hayward for suggestions that improved the manuscript. MV acknowledges support through NASA ATP 19-ATP19-0019, 19-ATP19-0020, 19-ATP19-0167, and NSF grants AST-1814053, AST-1814259, AST-1909831, AST-2007355 and AST-2107724. MBK acknowledges support from NSF CAREER award AST-1752913, NSF grants AST-1910346 and

AST-2108962, NASA grant 80NSSC22K0827, and HST-AR-15809, HST-GO-15658, HST-GO-15901, HST-GO-15902, HST-AR-16159, HST-GO-16226, HST-GO-16686, HST-AR-17028, and HST-AR-17043 from the Space Telescope Science Institute, which is operated by AURA, Inc., under NASA contract NAS5-26555.

DATA AVAILABILITY

The data underlying this article can be shared on reasonable request to the corresponding author. The source code and the observational data compiled for this project are publically available at [the online repository](#).

REFERENCES

- Adams N. J., et al., 2023a, *arXiv e-prints*, p. [arXiv:2304.13721](#)
- Adams N. J., et al., 2023b, *MNRAS*, **518**, 4755
- Anglés-Alcázar D., Faucher-Giguère C.-A., Kereš D., Hopkins P. F., Quataert E., Murray N., 2017, *MNRAS*, **470**, 4698
- Arrabal Haro P., et al., 2023a, *arXiv e-prints*, p. [arXiv:2303.15431](#)
- Arrabal Haro P., et al., 2023b, *arXiv e-prints*, p. [arXiv:2304.05378](#)
- Atek H., et al., 2023, *MNRAS*, **519**, 1201
- Behroozi P., Wechsler R. H., Hearin A. P., Conroy C., 2019, *MNRAS*, **488**, 3143
- Behroozi P., et al., 2020, *MNRAS*, **499**, 5702
- Bond J. R., Cole S., Efstathiou G., Kaiser N., 1991, *ApJ*, **379**, 440
- Bournaud F., Elmegreen B. G., Elmegreen D. M., 2007, *The Astrophysical Journal*, **670**, 237
- Bouwens R. J., et al., 2014, *ApJ*, **793**, 115
- Bouwens R. J., Illingworth G. D., Oesch P. A., Caruana J., Holwerda B., Smit R., Wilkins S., 2015, *ApJ*, **811**, 140
- Bouwens R., et al., 2020, *ApJ*, **902**, 112
- Bouwens R. J., et al., 2021, *AJ*, **162**, 47
- Bouwens R. J., et al., 2023a, *MNRAS*,
- Bouwens R., Illingworth G., Oesch P., Stefanon M., Naidu R., van Leeuwen I., Magee D., 2023b, *MNRAS*,
- Bowler R. A. A., Jarvis M. J., Dunlop J. S., McLure R. J., McLeod D. J., Adams N. J., Milvang-Jensen B., McCracken H. J., 2020, *MNRAS*, **493**, 2059
- Boylan-Kolchin M., 2023, *Nature Astronomy*, pp 10.1038/s41550-023-01937-7
- Boylan-Kolchin M., Springel V., White S. D. M., Jenkins A., Lemson G., 2009, *MNRAS*, **398**, 1150
- Broussard A., et al., 2019, *ApJ*, **873**, 74
- Bryan G. L., Norman M. L., 1998, *ApJ*, **495**, 80
- Bunker A. J., et al., 2023, *arXiv e-prints*, p. [arXiv:2302.07256](#)
- Caplar N., Tacchella S., 2019, *MNRAS*, **487**, 3845
- Carniani S., et al., 2018, *MNRAS*, **478**, 1170
- Castellano M., et al., 2022, *ApJ*, **938**, L15
- Ceverino D., Dekel A., Bournaud F., 2010, *MNRAS*, **404**, 2151
- Chabrier G., 2003, *PASP*, **115**, 763
- Chen Y., Mo H. J., Wang K., 2023, *arXiv e-prints*, p. [arXiv:2304.13890](#)
- Cochrane R. K., et al., 2019, *MNRAS*, **488**, 1779
- Coe D., et al., 2013, *ApJ*, **762**, 32
- Cullen F., et al., 2023, *MNRAS*, **520**, 14
- Curtis-Lake E., et al., 2023, *Nature Astronomy*,
- Davé R., Anglés-Alcázar D., Narayanan D., Li Q., Rafieferantsoa M. H., Appleby S., 2019, *MNRAS*, **486**, 2827
- Dayal P., Ferrara A., Dunlop J. S., Pacucci F., 2014, *MNRAS*, **445**, 2545
- Dayal P., Rossi E. M., Shiralilou B., Piana O., Choudhury T. R., Volonteri M., 2019, *MNRAS*, **486**, 2336
- Dekel A., Sari R., Ceverino D., 2009, *ApJ*, **703**, 785
- Dekel A., Sarkar K. C., Birnboim Y., Mandelker N., Li Z., 2023, *MNRAS*, **523**, 3201
- Dong F., Zhao D., Han J., Li Z., Jing Y., Yang X., 2022, *ApJ*, **929**, 120
- Donnan C. T., et al., 2023, *MNRAS*, **518**, 6011
- El-Badry K., Wetzel A., Geha M., Hopkins P. F., Kereš D., Chan T. K., Faucher-Giguère C.-A., 2016, *ApJ*, **820**, 131
- Ellis R. S., et al., 2013, *ApJ*, **763**, L7
- Elmegreen B. G., Elmegreen D. M., Fernandez M. X., Lemonias J. J., 2009, *ApJ*, **692**, 12
- Emami N., Siana B., Weisz D. R., Johnson B. D., Ma X., El-Badry K., 2019, *ApJ*, **881**, 71
- Endsley R., Stark D. P., Whittler L., Topping M. W., Chen Z., Plat A., Chisholm J., Charlot S., 2023, *MNRAS*, **524**, 2312
- Faisst A. L., Capak P. L., Emami N., Tacchella S., Larson K. L., 2019, *ApJ*, **884**, 133
- Fakhouri O., Ma C.-P., Boylan-Kolchin M., 2010, *MNRAS*, **406**, 2267
- Faucher-Giguère C.-A., 2018, *MNRAS*, **473**, 3717
- Ferrara A., et al., 2022, *MNRAS*, **512**, 58
- Ferrara A., Pallottini A., Dayal P., 2023, *MNRAS*, **522**, 3986
- Finkelstein S. L., et al., 2022, *ApJ*, **940**, L55
- Finkelstein S. L., et al., 2023, *ApJ*, **946**, L13
- Fiore F., Ferrara A., Bischetti M., Feruglio C., Travascio A., 2023, *ApJ*, **943**, L27
- Flores Velázquez J. A., et al., 2021, *MNRAS*, **501**, 4812
- Förster Schreiber N. M., et al., 2011, *ApJ*, **731**, 65
- Fujimoto S., et al., 2022, *arXiv e-prints*, p. [arXiv:2211.03896](#)
- Harikane Y., et al., 2018, *PASJ*, **70**, S11
- Harikane Y., et al., 2022, *ApJS*, **259**, 20
- Harikane Y., Nakajima K., Ouchi M., Umeda H., Isobe Y., Ono Y., Xu Y., Zhang Y., 2023a, *arXiv e-prints*, p. [arXiv:2304.06658](#)
- Harikane Y., et al., 2023b, *ApJS*, **265**, 5
- Haslbauer M., Kroupa P., Zonoozi A. H., Haghi H., 2022, *ApJ*, **939**, L31
- Hopkins P. F., et al., 2023, *MNRAS*,
- Howlett C., Lewis A., Hall A., Challinor A., 2012, *J. Cosmol. Astropart. Phys.*, **1204**, 027
- Inayoshi K., Harikane Y., Inoue A. K., Li W., Ho L. C., 2022, *ApJ*, **938**, L10
- Iyer K. G., et al., 2020, *MNRAS*, **498**, 430
- Iyer K. G., Speagle J. S., Caplar N., Forbes J. C., Gawiser E., Leja J., Tacchella S., 2022, *arXiv e-prints*, p. [arXiv:2208.05938](#)
- Kannan R., Garaldi E., Smith A., Pakmor R., Springel V., Vogelsberger M., Hernquist L., 2022, *MNRAS*, **511**, 4005
- Kannan R., et al., 2023, *MNRAS*, **524**, 2594
- Keller B. W., Munshi F., Trebitsch M., Tremmel M., 2023, *ApJ*, **943**, L28
- Labbé I., et al., 2023, *Nature*, **616**, 266
- Larson R. L., et al., 2022, *arXiv e-prints*, p. [arXiv:2211.10035](#)
- Leethochawalit N., et al., 2023, *ApJ*, **942**, L26
- Leitherer C., et al., 1999, *ApJS*, **123**, 3
- Lewis A., Challinor A., Lasenby A., 2000, *ApJ*, **538**, 473
- Lovell C. C., Harrison I., Harikane Y., Tacchella S., Wilkins S. M., 2023, *MNRAS*, **518**, 2511
- Madau P., Dickinson M., 2014, *ARA&A*, **52**, 415
- Mason C. A., Trenti M., Treu T., 2015, *The Astrophysical Journal*, **813**, 21
- Mason C. A., Trenti M., Treu T., 2023, *MNRAS*, **521**, 497
- Mauerhofer V., Dayal P., 2023, *arXiv e-prints*, p. [arXiv:2305.01681](#)
- McCaffrey J., Hardin S., Wise J., Regan J., 2023, *arXiv e-prints*, p. [arXiv:2304.13755](#)
- McLeod D. J., McLure R. J., Dunlop J. S., 2016, *MNRAS*, **459**, 3812
- McLeod D. J., et al., 2023, *arXiv e-prints*, p. [arXiv:2304.14469](#)
- Meurer G. R., Heckman T. M., Calzetti D., 1999, *ApJ*, **521**, 64
- Mirocha J., Furlanetto S. R., 2023, *MNRAS*, **519**, 843
- Mirocha J., La Plante P., Liu A., 2021, *MNRAS*, **507**, 3872
- Morishita T., Stiavelli M., 2023, *ApJ*, **946**, L35
- Morishita T., et al., 2018, *ApJ*, **867**, 150
- Moster B. P., Somerville R. S., Maulbetsch C., van den Bosch F. C., Macciò A. V., Naab T., Oser L., 2010, *ApJ*, **710**, 903
- Murphy E. J., et al., 2011, *ApJ*, **737**, 67
- Murray S., 2014, HMF: Halo Mass Function calculator, Astrophysics Source Code Library, record ascl:1412.006 (ascl:1412.006)
- Murray S. G., Power C., Robotham A. S. G., 2013, *Astronomy and Computing*, **3**, 23
- Naidu R. P., et al., 2022a, *arXiv e-prints*, p. [arXiv:2208.02794](#)

- Naidu R. P., et al., 2022b, *ApJ*, **940**, L14
- Nath B. B., Vasiliev E. O., Drozdov S. A., Shchekinov Y. A., 2023, *MNRAS*, **521**, 662
- Oesch P. A., Bouwens R. J., Illingworth G. D., Labbé I., Stefanon M., 2018, *ApJ*, **855**, 105
- Pallottini A., Ferrara A., 2023, *arXiv e-prints*, p. [arXiv:2307.03219](https://arxiv.org/abs/2307.03219)
- Papovich C., et al., 2023, *ApJ*, **949**, L18
- Pérez-González P. G., et al., 2023, *ApJ*, **951**, L1
- Planck Collaboration et al., 2020, *A&A*, **641**, A6
- Popesso P., et al., 2023, *MNRAS*, **519**, 1526
- Prada F., Behroozi P., Ishiyama T., Klypin A., Pérez E., 2023, *arXiv e-prints*, p. [arXiv:2304.11911](https://arxiv.org/abs/2304.11911)
- Press W. H., Schechter P., 1974, *ApJ*, **187**, 425
- Ren K., Trenti M., Mutch S. J., 2018, *ApJ*, **856**, 81
- Ren K., Trenti M., Mason C. A., 2019, *The Astrophysical Journal*, **878**, 114
- Robertson B. E., et al., 2023, *Nature Astronomy*,
- Rodríguez-Puebla A., Primack J. R., Behroozi P., Faber S. M., 2016, *MNRAS*, **455**, 2592
- Rogers A. B., et al., 2014, *MNRAS*, **440**, 3714
- Salpeter E. E., 1955, *ApJ*, **121**, 161
- Sheth R. K., Mo H. J., Tormen G., 2001, *MNRAS*, **323**, 1
- Smit R., Bouwens R. J., Labbé I., Franx M., Wilkins S. M., Oesch P. A., 2016, *ApJ*, **833**, 254
- Sparre M., Hayward C. C., Feldmann R., Faucher-Giguère C.-A., Muratov A. L., Kereš D., Hopkins P. F., 2017, *MNRAS*, **466**, 88
- Speagle J. S., Steinhardt C. L., Capak P. L., Silverman J. D., 2014, *ApJS*, **214**, 15
- Springel V., et al., 2005, *Nature*, **435**, 629
- Stefanon M., et al., 2019, *ApJ*, **883**, 99
- Steinhardt C. L., Kokorev V., Rusakov V., Garcia E., Sneppen A., 2023, *ApJ*, **951**, L40
- Sun G., Furlanetto S. R., 2016, *MNRAS*, **460**, 417
- Sun G., Faucher-Giguère C.-A., Hayward C. C., Shen X., Wetzel A., Cochrane R. K., 2023, *arXiv e-prints*, p. [arXiv:2307.15305](https://arxiv.org/abs/2307.15305)
- Tacchella S., Trenti M., Carollo C. M., 2013, *ApJ*, **768**, L37
- Tacchella S., Dekel A., Carollo C. M., Ceverino D., DeGraf C., Lapiner S., Mandelker N., Primack Joel R., 2016, *MNRAS*, **457**, 2790
- Tacchella S., Bose S., Conroy C., Eisenstein D. J., Johnson B. D., 2018, *The Astrophysical Journal*, **868**, 92
- Tacchella S., Forbes J. C., Caplar N., 2020, *MNRAS*, **497**, 698
- Tan J. C., 2000, *ApJ*, **536**, 173
- Tasker E. J., 2011, *ApJ*, **730**, 11
- Tinker J. L., Robertson B. E., Kravtsov A. V., Klypin A., Warren M. S., Yepes G., Gottlöber S., 2010, *ApJ*, **724**, 878
- Topping M. W., Stark D. P., Endsley R., Plat A., Whitler L., Chen Z., Charlot S., 2022, *ApJ*, **941**, 153
- Trenti M., Stiavelli M., 2008, *ApJ*, **676**, 767
- Treu T., et al., 2023, *ApJ*, **942**, L28
- Vogelsberger M., et al., 2020, *MNRAS*, **492**, 5167
- Whitler L. R., Mason C. A., Ren K., Dijkstra M., Mesinger A., Pentericci L., Trenti M., Treu T., 2020, *MNRAS*, **495**, 3602
- Wilkins S. M., et al., 2023a, *MNRAS*, **518**, 3935
- Wilkins S. M., et al., 2023b, *MNRAS*, **519**, 3118
- Yan H., Ma Z., Ling C., Cheng C., Huang J.-S., 2023, *ApJ*, **942**, L9
- Yung L. Y. A., Somerville R. S., Finkelstein S. L., Popping G., Davé R., 2019, *MNRAS*, **483**, 2983
- Yung L. Y. A., Somerville R. S., Finkelstein S. L., Wilkins S. M., Gardner J. P., 2023, *arXiv e-prints*, p. [arXiv:2304.04348](https://arxiv.org/abs/2304.04348)
- Zavala J. A., et al., 2023, *ApJ*, **943**, L9
- Ziparo F., Ferrara A., Sommovigo L., Kohandel M., 2023, *MNRAS*, **520**, 2445

This paper has been typeset from a $\text{\TeX}/\text{\LaTeX}$ file prepared by the author.